Published in final edited form as:
Clin Cancer Res. 2011 December 1; 17(23): 7359–7372. doi:10.1158/1078-0432.CCR-11-1388.

Preclinical Testing of PI3K/AKT/mTOR Signaling Inhibitors in a Mouse Model of Ovarian Endometrioid Adenocarcinoma

Rong Wu[1], **Tom C. Hu**[1], **Alnawaz Rehemtulla**[2,4], **Eric R. Fearon**[1,3,4], and **Kathleen R. Cho**[1,3,4]

[1]Department of Pathology, The University of Michigan Medical School, Ann Arbor, Michigan 48109

[2]Department of Radiation Oncology, The University of Michigan Medical School, Ann Arbor, Michigan 48109

[3]Department of Internal Medicine, The University of Michigan Medical School, Ann Arbor, Michigan 48109

[4]Comprehensive Cancer Center, The University of Michigan Medical School, Ann Arbor, Michigan 48109

Abstract

Purpose—Genetically engineered mouse (GEM) models of ovarian cancer that closely recapitulate their human tumor counterparts may be invaluable tools for preclinical testing of novel therapeutics. We studied murine ovarian endometrioid adenocarcinomas (OEAs) arising from conditional dysregulation of canonical WNT and PI3K/AKT/mTOR pathway signaling to investigate their response to conventional chemotherapeutic drugs and mTOR or AKT inhibitors.

Experimental Design—OEAs were induced by injection of adenovirus expressing Cre recombinase (AdCre) into the ovarian bursae of $Apc^{flox/flox};Pten^{flox/flox}$ mice. Tumor-bearing mice or murine OEA-derived cell lines were treated with cisplatin and paclitaxel, mTOR inhibitor rapamycin, or AKT inhibitors API-2 or perifosine. Treatment effects were monitored in vivo by tumor volume and bioluminescence imaging, in vitro by WST-1 proliferation assays, and in OEA tissues and cells by immunoblotting and immunostaining for levels and phosphorylation status of PI3K/AKT/mTOR signaling pathway components.

Results—Murine OEAs developed within 3 weeks of AdCre injection and were not preceded by endometriosis. OEAs responded to cisplatin + paclitaxel, rapamycin, and AKT inhibitors in vivo. In vitro studies showed that response to mTOR and AKT inhibitors, but not conventional cytotoxic drugs, was dependent on the status of PI3K/AKT/mTOR signaling. AKT inhibition in $APC^{-}/PTEN^{-}$ tumor cells resulted in compensatory up-regulation of ERK signaling.

Conclusion—The studies demonstrate the utility of this GEM model of ovarian cancer for pre-clinical testing of novel PI3K/AKT/mTOR signaling inhibitors and provide evidence for compensatory signaling, suggesting that multiple rather than single agent targeted therapy will be more efficacious for treating ovarian cancers with activated PI3K/AKT/mTOR signaling.

Keywords

ovarian carcinoma; endometriosis; PI3K/AKT/mTOR signaling; mouse model; bioluminescence imaging

*Correspondence: Kathleen R. Cho, M.D., Department of Pathology, University of Michigan Medical School, 1506 BSRB, 109 Zina Pitcher, Ann Arbor, MI 48109-2200 Tel. 734-764-1549; FAX 734-647-7950; kathcho@umich.edu.

INTRODUCTION

More than two-thirds of women diagnosed with ovarian carcinoma present with advanced stage disease, and their overall 5-year survival is only 28% (1, 2). Although the initial response of ovarian carcinomas to standard therapy (surgical debulking and chemotherapy with platinum-based drugs and taxanes) is often excellent, relapse with drug-resistant cancer usually occurs and patients succumb to their disease. Over the last several years, much progress has been made in identifying "hallmark" genetic lesions associated with each major subtype of ovarian carcinoma. Novel therapeutics that target the signaling pathways dysregulated as a result of these molecular defects are being developed, with the hope that "individualized" therapeutic regimens based on the specific molecular defects present in a given patient's tumor could be used alone or in combination with existing cytotoxic agents to improve clinical outcome.

Surgical pathologists continue to employ morphology-based schemes for classifying ovarian carcinomas (OvCas) based largely on their degree of resemblance to non-neoplastic epithelia in the female genital tract. However, mounting clinico-pathologic and molecular data have led Kurman and Shih to propose a new model in which OvCas are divided into two main categories - Type I and Type II (3–5). Type I OvCas are suggested to be low-grade, relatively indolent and genetically stable tumors that arise from well-defined precursor lesions such as endometriosis or so-called borderline tumors, and frequently harbor somatic mutations that dysregulate certain cell signaling pathways (e.g., *KRAS, BRAF, CTNNB1, PTEN*). Type I OvCas include most endometrioid, clear cell, and mucinous carcinomas and low-grade serous carcinomas. In contrast, Type II OvCas are proposed to be high-grade, biologically aggressive tumors from their outset, with a propensity for metastasis from small-volume primary lesions. Most Type II OvCas are high-grade serous carcinomas, virtually all of which harbor mutant *TP53* alleles (6).

Genetic alterations that dysregulate the canonical Wnt (i.e., Wnt/β-catenin/Tcf) and PI3K/Akt/mTOR signaling pathways often occur together in human ovarian endometrioid adenocarcinoma (OEA) (7, 8). Given substantial overlap in the molecular features (gene expression and mutational profiles) of tumors diagnosed as high grade OEAs, with high grade serous carcinomas (7), some pathologists default the majority of gland-forming or near-solid cytologically high-grade carcinomas to the serous category, and consider "true" high-grade OEAs to be rare or non-existent (9). If only low grade (prototypical Type I) OEAs are considered, the majority have mutations predicted to dysregulate canonical Wnt and/or PI3K/Akt/mTOR signaling and *TP53* is usually wild type. Loss of function mutations in *ARID1A* (which encodes the AT-rich interactive domain-containing protein 1A) have also been recently reported in 30% of OEAs (10). Given the frequency with which Wnt and PI3K/Akt/mTOR signaling is activated in OEAs, drugs that target these pathways might prove to be particularly useful for treating patients with advanced-stage disease or in the adjuvant setting for patients with OEA who might be at risk of recurrence. Given our limited ability to exhaustively test multiple drug combinations, doses, and schedules in clinical trials, it is anticipated that animal models which closely mimic their human disease counterparts will provide an invaluable tool for the identification of multi-drug regimens with greatest promise for efficacy in humans.

We previously described a murine model of (Type I) OEA based on conditional inactivation of the *Apc* and *Pten* tumor suppressor genes following injection of adenovirus expressing Cre recombinase (AdCre) into the ovarian bursae of $Apc^{flox/flox}$; $Pten^{flox/flox}$ mice (7). Several characteristics of this mouse model suggest its relevance and tractability for testing novel therapeutic approaches. First, complicated breeding schemes are not needed to generate mice with the appropriate genotype once a breeding colony has been established.

Second, tumors invariably arise within a few weeks following AdCre injection, and recapitulate the morphology and gene expression pattern of human OEAs with comparable signaling pathway defects. Third, tumors arise in the ovary and in immunologically intact animals, so possible effects of the tumor microenvironment on therapeutic response can be assessed. Finally, similar to women with advanced ovarian cancer, three quarters of the mice develop hemorrhagic ascites, and nearly one quarter acquire overt peritoneal dissemination. To demonstrate this model's utility for pre-clinical testing of novel therapeutics targeting the PI3K/Akt/mTOR signaling pathway, we pursued proof-of-principle studies demonstrating the response of murine OEAs to conventional chemotherapeutic drugs (cisplatin and paclitaxel) and mTOR and AKT inhibitors in vitro and in vivo. Additionally, we demonstrate the application of a Cre-inducible luciferase reporter allele for longitudinal in vivo monitoring of tumor development and drug response in the mice.

MATERIALS AND METHODS

Mouse strains and tumor induction

Apc$^{flox/flox}$; *Pten*$^{flox/flox}$ mice and ovarian bursal delivery of replication-incompetent recombinant adenovirus expressing Cre recombinase (AdCre) have been described previously in detail (7). Briefly, Cre-mediated recombination in these animals results in a frameshift mutation at *Apc* codon 580 (11), and the deletion of exons 4 and 5 of *Pten* (12). For tumor induction, 5×10^7 plaque-forming units (p.f.u.) of AdCre (purchased from the University of Michigan's Vector Core) with 0.1% Evans Blue (Sigma-Aldrich Inc., St. Louis, MO) were injected into the right ovarian bursal cavities of 2–5 month old female mice. In each mouse, the left ovarian bursa was not injected and served as control. Six weeks following AdCre injection, cohorts of mice were randomly assigned to drug treatment or vehicle control groups unless otherwise specified. Animals were euthanized by CO_2 asphyxiation following 3–4 weeks of drug treatment. All animal studies were performed under a protocol approved by the University of Michigan's University Committee on Use and Care of Animals.

Cell Lines

W2671T and W2830T cell lines were generated from APC$^-$/PTEN$^-$ murine ovarian tumors. Briefly, fresh ovarian tumor tissues were mechanically minced with sterile scalpels and further digested at 37°C with 0.05% Trypsin-EDTA for 20 minutes. Cells were cultured for five passages in DMEM containing 10% FBS/1% Penicillin/Streptomycin (P/S)/1% Insulin-Transferrin-Selenium (Invitrogen) in an incubator with 3% O_2/5% CO_2 (Model NAPCO 8000WJ, Thermal Scientific, Asheville, NC). Cells were maintained in DMEM supplemented with 10% FBS/1% P/S in a standard 5% CO2 incubator (Model 3307, Thermo Scientific). ID8 cells (spontaneously transformed ovarian surface epithelial cells from a C57B/L6 mouse) were obtained from KF Roby (University of Kansas Medical Center, Kansas City, KS) (13). The human OEA-derived cell line TOV-112D and ovarian carcinoma cell line A2780 were obtained from the American Type Culture Collection (ATCC, Rockville, MD). TOV-112D cells harbor an activating (S37A) *CTNNB1* mutation (14), but lack known PI3K/AKT/mTOR pathway defects. A2780 has biallelic inactivation of *PTEN* (9bp deletion in exon 5 and 37bp deletion in exon 8) but lacks known canonical Wnt pathway defects (15). To generate human ovarian carcinoma cells with dysregulation of both PI3K/Akt/mTOR and Wnt signaling, we transduced A2780 cells with a mutant (oncogenic) form of β-catenin (S33Y) by infecting cells with S33Y β-catenin-expressing retroviruses or control (PGS-CMV-CITE-neo) (16).

Drugs and treatment in mice

Rapamycin (LC Laboratories, Woburn, MA) was reconstituted in 100% ethanol at 10mg/ml, stored at −30°C and diluted in 5% Tween-80 and 5% PEG-400 before injection. Rapamycin was injected intraperitoneally (IP) at concentrations of 4mg/kg (n=5) or 1mg/kg (n=8) in a final volume of 100 μl, 3 times weekly for 4 weeks. API-2 (Calbiochem, Gibbstown, NJ) in 5% DMSO was injected IP at a dose of 1mg/kg in 100 μl daily for 3–4 weeks. Control mice were treated with 5% DMSO alone. Perifosine in 0.9% NaCl (Cayman Chemical, Ann Arbor, MI) was given by oral gavage (125mg/kg, twice weekly) for 4 weeks. The control group was administered 0.9% NaCl orally in parallel. Cisplatin (LC Laboratories) in 0.9% NaCl (5mg/kg) and paclitaxel (LC Laboratories) in 5% DMSO (20mg/kg) were administered via IP injection, once a week for 4 weeks. Cisplatin and paclitaxel were administered on the same day, with paclitaxel being given 20 minutes after cisplatin. Control mice were given 0.9% NaCl first, then 5% DMSO.

WST-1 cell proliferation assay

WST-1 assays for cell proliferation were performed per the manufacturer's instructions (Roche Applied Science, Pleasanton, CA). Briefly, $1\sim2\times10^4$ cells were plated in each well of 96-well plates and cultured overnight. After addition of drugs, cells were incubated for another 24 hr. Cell proliferation reagent (10 μl per well) was then added and cells were incubated for another 2–3 hr. Absorbance of the samples at 450 and 600nm was measured with a 96-well spectrophotometric plate reader (SpectraMax 190, Molecular Devices, Sunnyvale, CA). Effects of drug treatments on cell proliferation were evaluated using one-way ANOVA (GraphPad Prism, version 5.01 GraphPad Software, Inc., La Jolla, CA).

Immunoblotting

Cultured cells were treated with rapamycin (0.01–100nM) or API-2 (40 μM) for up to 24 hr or with perifosine (40–80 μM) for 2 hr. Whole cell protein lysates were then prepared in RIPA buffer (Radio-Immunoprecipitation Assay) containing Complete™ Protease Inhibitor Cocktail Tablets (Roche) and Phosphatase inhibitor cocktails (Sigma). Immunoblotting was performed using standard protocols. Total protein lysates (30–50 μg) were separated on NuPage 4–12% Bis-Tris precast gels (Invitrogen) and then transferred to Immobilon-P membranes (Millipore, Bedford, MA). Antibody complexes were detected with enhanced chemiluminescent reagents (PerkinElmer, Waltham, MA) and exposed to HyBlot CL film (Denville Scientific Inc., South Plainfield NJ).

Histopathology and immunohistochemistry

After drug treatment, all mice were euthanized and examined at necropsy for gross organ abnormalities. The genital tract and other major organs were collected, fixed in 10% (v/v) buffered formalin, embedded in paraffin, and processed for staining with hematoxylin and eosin (H&E). Histopathological evaluation of tumor and other tissues was performed by a surgical pathologist with expertise in gynecologic cancer diagnosis (K.R.C). Immunohistochemical (IHC) staining was performed on formalin-fixed, paraffin-embedded tissues or frozen sections using standard methods. For mouse primary antibodies, mouse on mouse kit (M.O.M., Vector Laboratories Inc., Burlingame, CA) was used to reduce nonspecific staining per the manufacturer's instructions. Immunofluorescence (IF) staining was carried out as previously described (14). Briefly, cells were grown in chamber slides for 2 days, then fixed with 4% paraformaldehyde for 20 min and permeabilized with 1% goat serum/0.5% Triton X-100/PBS for 15 min at room temperature. After washing with PBS, slides were blocked with 2% goat serum/0.2% TritonX-100/PBS for 60 min. Cells were incubated with primary antibody at 4°C overnight. After washing with PBS, cells were incubated with Alexa 594 Red-conjugated secondary antibody at a dilution of 1:1000 for 60

min at room temperature. Slides were washed with PBS and then counterstained with Hoechst (1:1000) for 5 min. Prolong Gold antifade reagent (Fisher) was used to mount the coverslips.

Antibodies

The following primary antibodies were used for IHC or IF staining: Mouse anti-β-catenin (Transduction laboratories, Lexington, KY); Mouse anti-α-inhibin (Serotac Ltd, Oxford, UK); Rat anti-cytokeratin 8 (CK8, #TROMA 1, Developmental Studies Hybridoma Bank, University of Iowa, Iowa City, IA); Rat anti-Ki67 (clone TEC-3, Dako, Carpinteria, CA); Rabbit anti-pten (clone 138G6, Cell Signaling, Boston, MA, #9559); Rabbit anti-cleaved caspase-3 (Asp175) Cell Signaling, #9661); Rabbit anti-phospho-S6 Ribosomal Protein (Ser235/236) (Cell Signaling, #4857); and mouse anti-CD10 (Novocastra, UK, #NCL-CD-270). Antibodies used for immunoblotting were: Rabbit anti-phospho-AKT (Ser473) (Cell Signaling #4060); Rabbit anti-AKT (Cell Signaling #9272); Mouse anti-phospho-ERK (E-4) (Santa Cruz #7383); Rabbit anti-ERK1/2 (Cell Signaling #9102); Rabbit anti-phospho-S6 Ribosomal Protein(Ser235/236) (Cell Signaling #4857); Mouse anti-S6 Ribosomal Protein (Cell Signaling #2317); Rabbit anti phospho-p70 S6 (Thr389) kinase (Cell Signaling #9205); Rabbit anti-p70 S6 kinase (Santa Cruz #SC-230); Rabbit anti-phospho-4E-BP1 (Thr70) (Cell Signaling #9455); Rabbit anti-phospho-4E-BP1 (Thr37/46) (Cell Signaling #2855); Rabbit anti-4E-BP1 (Cell signaling #9644); Mouse anti-active β-catenin (Clone 8E7, Millipore); Rabbit anti-phospho-GSK3β(Ser9) Cell Signaling #9323); and Rabbit anti-GSK3β(Cell Signaling #9315).

In vivo bioluminescence imaging (BLI)

The mouse luciferase reporter strain *Rosa26*$^{L\text{-}S\text{-}L\text{-}Luc/+}$ (17) was purchased from the Jackson Laboratory (stock #005125, Bar Harbor, ME). Luciferase expression in the mouse ovarian surface epithelium (MOSE) was induced by ovarian intrabursal injection of AdCre. Mice were imaged using an IVIS Image System 200 Series (Xenogen Corporation, Alameda, CA, USA). During the imaging procedure, mice were anaesthetized with a constant flow of 1.5% isoflurane from the IVIS manifold and then administered a single IP dose of D-luciferin (150 mg/kg, Biosynth International, Inc. Itasca IL) in a volume of 100 μl in normal saline. Image acquisition was initiated approximately 10 min after injection of D-luciferin. The bioluminescence signals (photons/s) emitted from the mice were collected using sequential mode until reaching peak values and analyzed by LivingImage 3.0 software (Xenogen Corporation). For studies of tumor-bearing animals, *Rosa26*$^{L\text{-}S\text{-}L\text{-}Luc/+}$ and *Apc*$^{flox/flox}$; *Pten*$^{flox/flox}$ mice were crossed to generate *Apc*$^{flox/flox}$; *Pten*$^{flox/flox}$; *Rosa26*$^{L\text{-}S\text{-}L\text{-}luc/+}$ mice. After baseline imaging 6 weeks after AdCre infection, mice were treated with either drug or vehicle. Treated mice were then re-imaged at weekly intervals for 4 weeks. For each animal, bioluminescence was normalized to its baseline (before treatment, 0 week) and signals were adjusted to the same color scale for the entire time course.

RESULTS

Temporal analysis of ovarian murine tumor development following AdCre injection

Our previous studies have shown that mice bearing APC^{-}/PTEN^{-} tumors survive 11–12 weeks on average (range 7–19 weeks) after injection of AdCre. To assess the possible value of this model for studying effects of chemoprevention or early intervention, we sought to define the earliest time point at which OEAs or precursor lesions could be detected. Cohorts of *Apc*$^{flox/flox}$; *Pten*$^{flox/flox}$ mice (total n=43) were evaluated weekly from one to six weeks after ovarian bursal AdCre injection. Mice were euthanized and their genital tracts evaluated for gross and microscopic lesions; data are summarized in Table 1. No gross or microscopic lesions were detectable in any of the mice examined at one (n=2) or two (n=8) weeks after

AdCre injection. In 6 of 10 mice euthanized after three weeks, microscopic dysplastic lesions were found exclusively in the injected (right) ovaries (Figure 1A, B). Multifocal aggregates of epithelial cells ("tumorlets"), morphologically indistinguishable from those seen in well-established tumors, were present on the ovarian surface. Based on IHC staining, cells in the surface tumorlets were cytokeratin 8-positive (Figure 1C) and α-inhibin-negative (Figure 1D), consistent with epithelial differentiation. As expected, the tumor cells also showed strong nuclear expression of β-catenin (Figure 1E) and absence of PTEN expression (Figure 1F). In 13 mice euthanized 6 weeks post-AdCre injection, 2 had microscopic ovarian tumorlets and 11 had grossly visible, small ovarian tumors (Figure 1G); none had developed ascites or peritoneal metastasis. Microscopically, the 6-week tumors showed areas of overt glandular differentiation (Figure 1H) admixed with more poorly differentiated and spindle cell areas as observed in the more advanced tumors we described previously (7).

Development of APC^{-}/PTEN^{-} murine ovarian tumors is not preceded by endometriosis

A substantial proportion of human ovarian carcinomas with endometrioid or clear cell differentiation are believed to arise from endometriosis (18). Notably, we did not observe endometriosis-like lesions in any of the 43 *Apc*$^{flox/flox}$*; Pten*$^{flox/flox}$ mice evaluated 1–6 weeks following AdCre injection or, in our previous study, in mice with well-established APC^{-}/PTEN^{-} tumors (7). After ovarian bursal injection of AdCre, groups of mice where only the *Apc* (*Apc*$^{flox/flox}$) or *Pten* (*Pten*$^{flox/flox}$) genes were individually inactivated were monitored for 12–13 months for tumor development. No ovarian epithelial tumors were found in either group, though benign endometrial-type glands and stroma morphologically similar to endometriosis were observed at the end of the monitoring period in the injected (right) ovaries in 9 of 49 *Apc*$^{flox/flox}$ mice. Similar lesions were identified in the uninjected (left) ovaries of 6 mice (Figure 2A, B). In *Pten*$^{flox/flox}$ control mice (n=47), endometriosis was observed in one AdCre injected ovary. We did not observe tumor formation or endometriosis lesions in any of 24 C57BL/6J mice monitored from 3 to 13 months following ovarian bursal AdCre injection. As expected for endometriosis, IHC staining showed strong CK8 positivity in the glandular epithelium and scattered CD10 positive cells in the adjacent endometriotic stroma (Figure 2C, D). Expression of α-inhibin was weak in the stroma relative to the granulosa cells in the ovarian follicles (Figure 2E). Importantly, the glandular epithelium showed exclusively membranous staining for β-catenin, indicating absence of Cre-mediated inactivation of *Apc*, even in the AdCre-injected ovaries (Figure 2F). This finding, in addition to our observation of endometriosis-like lesions in the uninjected as well as injected ovaries, suggests, but does not definitively prove, that the development of endometriosis in a subset of the mice is not dependent on Cre-mediated inactivation of *Apc* or *Pten*, but may instead reflect a background rate of endometriosis development that varies to some degree with the genetic background of the mice studied.

Status of PI3K/AKT/mTOR signaling in murine ovarian cancer cells determines response to AKT and mTOR inhibitors, but not to conventional cytotoxic drugs

The PI3K/AKT/mTOR signaling pathway plays an important role in the regulation of cell growth, proliferation, and survival by controlling the phosphorylation of several translation factors. We first wished to test effects of selected PI3K/AKT/mTOR pathway-targeted therapies and conventional cytotoxic agents on murine tumor cell proliferation in vitro. WST-1 proliferation assays were performed using three transformed murine ovarian surface epithelial cell lines. The W2671T and W2830T cell lines were established in our laboratory following primary culture of murine OEAs induced by AdCre injection in *Apc*$^{flox/flox}$*; Pten*$^{flox/flox}$ mice. These cells show epithelial-like cobblestone morphology in culture (Supplemental Figure S1 A, B). The cells are cytokeratin 8-(Supplemental Figure S1C) and E-cadherin-positive, and vimentin-negative (Supplemental Figure S1D) based on IF staining. ID8 cells, a spontaneously transformed mouse ovarian surface epithelial cell line

lacking known PI3K/AKT/mTOR and canonical WNT pathway defects, were also employed for our studies (13). Cells were incubated with different doses of drugs for 24 hr, and data were normalized to vehicle treatment. W2671T cells displayed profound dose-dependent growth inhibition in response to rapamycin, cisplatin, and paclitaxel (Figure 3A–C). More modest inhibitory effects were observed with perifosine, a synthetic alkyl phospho-lipid that targets cell membranes and inhibits PKB-mediated AKT activation (Figure 3D) (19). Statistically significant growth inhibition was observed in W2671T at the highest (40 μM) perifosine concentration. In contrast, ID8 cells were sensitive to cisplatin and paclitaxel but showed minimal response to rapamycin, and no response to perifosine, even at the highest concentrations. These results confirm differential sensitivity to drugs that target PI3K/AKT/mTOR signaling in murine ovarian cancer cells, depending on the presence or absence of PI3K/AKT/mTOR pathway defects in the cells.

Characterization of PI3K/AKT/mTOR signaling pathway regulation in murine and human ovarian cancer cells after rapamycin treatment in vitro

The serine/threonine protein kinase mTOR exists in two functional complexes, mTORC1 and mTORC2. mTORC1 is a major regulator of cell growth, containing mTOR, Raptor, and mLST8. mTORC1 phosphorylates ribosomal protein S6 kinase beta-1 (S6K1) at Thr389, which is necessary for activation and phosphorylation of the eukaryotic translation initiation factor 4E-binding protein 1 (4E-BP1). Phosphorylation of 4E-BP1 blocks its binding to eIF4E and results in increased translation of capped mRNAs. Phosphorylated S6K1 further phosphorylates ribosomal protein S6 (S6) to promote ribosome biogenesis. Rapamycin suppresses both cell proliferation and cell growth through inhibition of mTORC1 (20, 21). mTORC2, comprised of mTOR, Rictor, mSin1, and mLST8, is relatively resistant to rapamycin. mTORC2 regulates activation of Akt, and mTORC2 activity is stimulated by growth factors such as insulin and insulin growth factor-1 (IGF-1).

To further characterize the time and dose-dependent downstream effects of drug-target interactions in vitro, the status of several PI3K/AKT/mTOR signaling pathway components was evaluated in two murine OEA-derived cell lines (W2671T, W2830T) before and after rapamycin treatment. As expected, in the absence of drug treatment, W2671T and W2830T cells exhibited constitutive phosphorylation (p) of AKT (Ser473), S6K1 (Thr389), and S6 (Ser235/236). In contrast, there was no or very low level expression of pAKT, pS6K1, and pS6 in ID8 cells, which lack known PI3K/AKT/mTOR and Wnt signaling pathway defects (Figure 4A). Levels of p4E-BP1 were similarly low in all three cell lines. Several investigators have reported that 100–1000 nM rapamycin treatment can inhibit activation of endogenous mTOR (22, 23). Treatment of W2671T and W2830T cells with 100nM rapamycin over a 24 hr time course showed complete loss of pS6K1 by the 0.5 hr time point and loss of pS6 between 0.5 and 4 hr. The timing of pAKT loss in reponse to rapamycin varied between the two lines, but pAKT was undetectable in both lines by the 24 hr time point (Figure 4B). Levels of p4E-BP1 were largely unchanged by rapamycin treatment, in keeping with recent reports that combined inhibition of Akt and Erk signaling is required to suppress 4E-BP1 phosphorylation (24). In order to determine the minimal concentration of rapamycin needed to abolish pS6K1 and pS6 expression in our murine $APC^{-}/PTEN^{-}$ OEA cells, W2671T cells were treated for 2 hr with doses of rapamycin ranging from 0.01 to 100 nM. Expression of pS6K1 and pS6 was virtually undetectable with rapamycin concentrations as low as 0.1nM (Figure 4C). In contrast to W2671T cells treated with 100nM rapamycin (Figure 4B), cells treated with 1nM of rapamycin showed no change in AKT phosphorylation over a 24 hr time course (Figure 4D). At both the 1nM and 100nM rapamycin doses, early and sustained decreases in phosphorylation of both S6K1 and S6 were observed (Figure 4B, D). These findings suggest that, in our model system, low doses of rapamycin inhibit only mTORC1, while higher doses are able to inhibit both mTORC1

and mTORC2 in our model system. Interestingly, p4E-BP1 (Thr70) was elevated after 2 hr of low dose (1nM) rapamycin treatment, peaked at 4 hr, then gradually decreased and was completely inhibited at 24 hr (Figure 4D). p4E-BP1 (Thr37/46), the form with phosphorylation of the priming sites required for Thr70 phosphorylation, was increased between 0.5–16 hr and was nearly undetectable at 24 hr (Figure 4D). These changes in p4E-BP1 levels were not observed with the high dose (100 nM) of rapamycin (Figure 4B).

We wished to determine if rapamycin treatment yielded comparable effects in human ovarian cancer cells with canonical Wnt and/or PI3K/Akt/mTOR pathway defects. The TOV-112D cell line was derived from a human OEA and harbors mutant *CTNNB1* and wild-type *PTEN* alleles (14). As expected, TOV-112D cells expressed substantial levels of transcriptionally active β-catenin (dephosphorylated on Ser37 or Thr41) which were not affected by rapamycin. pAkt was undetectable at baseline and after 2 hr of treatment with rapamycin doses between 0.1 and 100 nM (Supplemental Figure S2A), and remained undetectable after 24 hr of treatment (data not shown). Expression of pS6K1 and pS6 was inhibited by treatment with rapamycin concentrations as low as 0.1–1.0 nM. p(Ser9)GSK3β was modestly inhibited by 1–100 nM rapamycin, consistent with GSK3β as a downstream target of Akt in cells with intact PI3K/Akt/mTOR signaling. A2780 ovarian carcinoma cells have biallelic inactivation of *PTEN* (15). These cells were transduced with a mutant (S33Y) form of β-catenin in order to generate a human ovarian cancer cell line with dysregulation of both Wnt and PI3K/AKT/mTOR signaling. As expected, and in contrast to TOV-112D cells, A2780 cells with and without mutant β-catenin show elevated pAkt at baseline (Supplemental Figure S2B). Effects of rapamycin on PI3K/Akt/mTOR pathway components were largely similar in the presence and absence of mutant β-catenin, indicating Wnt pathway defects do not significantly alter effects of rapamycin in ovarian cancer cells with dysregulated PI3K/Akt/mTOR signaling. Our data are also consistent with previous reports that phosphorylation of S6K and S6 is not regulated by β-catenin (25).

Growth of APC^{-}/PTEN^{-} murine OEAs is inhibited in vivo by conventional chemotherapy and drugs targeting activated PI3K/AKT/mTOR signaling

The response of mouse OEAs to AKT and/or mTOR inhibitors in vivo would help demonstrate the model's potential utility for testing novel drugs targeting activated PI3K/AKT/mTOR signaling. Because clinical trials in ovarian cancer patients would likely compare the activity of targeted agents to that of conventional cytotoxic chemotherapy, it would also be useful to know whether the murine APC^{-}/PTEN^{-} tumors respond to cisplatin/paclitaxel in vivo. We therefore tested tumor-bearing mice for response to rapamycin, a first-generation mTOR inhibitor that directly binds mTORC1, a downstream effector of activated AKT. Tumor response to "conventional" combination therapy with cisplatin and paclitaxel and two mechanistically distinct AKT inhibitors (API-2 and perifosine) was also evaluated. API-2 (Akt/protein kinase B signaling inhibitor-2), also known as triciribine, is a cell-permeable tricyclic nucleoside that selectively inhibits the cellular phosphorylation/activation of AKT (26), while perifosine targets cell membranes and inhibits PKB-mediated AKT activation (19). Perifosine has also been shown to facilitate degradation of mTOR signaling pathway components including mTOR, raptor, rictor, S6K, and 4E-BP1 (27).

For these experiments, AdCre was injected into the right ovarian bursa of *Apc*$^{flox/flox}$; *Pten*$^{flox/flox}$ mice and drug (or vehicle) treatment was initiated after 6 weeks, when all of the mice were expected to have developed at least small tumors based on the studies described above. Data collected after 4 weeks of treatment with rapamycin (two doses), API-2, perifosine and cisplatin/paclitaxel are shown in Figures 5A–D, respectively. Treatment with each regimen, including both low (1 mg/kg) and high (4 mg/kg) doses of rapamycin, resulted in statistically significant inhibition of tumor growth over 4 weeks based on measurements of tumor volume at necropsy. Microscopic analysis of H&E stained sections

showed that residual drug-treated tumors were morphologically similar to vehicle-treated tumors (data not shown). None of the drug-treated animals developed liver metastases during the treatment period (compared to three of the vehicle-treated mice), and only 2 of 36 (6%) drug-treated mice (both in the low-dose rapamycin group) developed ascites, compared to 12 of 33 (36%) vehicle-treated mice. These data are summarized in Table 2.

Effects of drug treatment on cell proliferation in the residual ovarian tumors were evaluated by IHC staining for Ki-67 in tumor tissue sections. The Ki-67 index was defined as the percentage of Ki-67 positive cells in the most cellular areas of tumor. Data from two 400X fields were collected and averaged. The Ki-67 index was significantly reduced in rapamycin-treated tumors (n=12) compared with vehicle-treated tumors (n=6) in control mice (28.03 ± 3.27% vs. 41.84 ± 4.82%, p=0.0418). The Ki-67 index was also lower in perifosine-treated tumors relative to vehicle-treated controls, but the difference did not achieve statistical significance (31.49 ± 1.61% vs. 46.15 ± 6.61%, p = 0.097). API-2 had no appreciable effect on the Ki-67 index (48.80 ± 5.41% vs. 42.21 ± 4.47%, p=.3747). Apoptosis in rapamycin vs. vehicle-treated tumors was evaluated by IHC staining for the active form of caspase-3, cleaved caspase-3 (CC3), using an antibody that recognizes the p20/p17 subunit in the cytoplasm of apoptotic cells. Only rare positive cells were identified in tissue sections from tumors treated with rapamycin or vehicle (data not shown), and no significant difference was noted between the two groups. This finding is consistent with previous reports that rapamycin and its analogs can sensitize tumor cells in culture to cisplatin-induced apoptosis, but have minimal effects on apoptosis when used alone (28). Effects of cisplatin and paclitaxel on tumor cell proliferation and apoptosis could not be analyzed because residual tumor was identified in only one of six treated animals. Immunoblotting and IHC staining were used to analyze residual $APC^{-}/PTEN^{-}$ tumors remaining after 4 weeks of treatment with rapamycin. Only small amounts of tumor tissue remained after treatment, limiting the number of studies that could be performed. We found that pS6 (Ser235/236) levels were lower, and pAKT levels slightly increased, in rapamycin-treated tumors compared to those receiving vehicle (Supplemental Figure S3, upper panel). IHC staining of residual tumor tissue confirmed significant reduction of pS6 in the rapamycin-treated tumors compared to controls (Supplemental Figure S3, lower panels).

Tumor imaging

The ability to non-invasively and quantitatively image localized and metastatic OEAs in live animals would permit repeated and accurate measurements of tumor burden, increasing statistical power and reducing the number of animals needed to test each therapeutic regimen. To demonstrate the feasibility of this approach, we further engineered our OEA model to include a luciferase reporter allele that can be activated by AdCre. Mice with a Cre-activatable form of firefly luciferase allele present at the ubiquitously expressed *Rosa26* locus were crossed with $Apc^{flox/flox};Pten^{flox/flox}$ mice to generate $Apc^{flox/flox};Pten^{flox/flox};ROSA26^{L\text{-}S\text{-}L\text{-}Luc/+}$ mice (17). We performed ovarian bursal injection of AdCre in $Apc^{flox/flox};Pten^{flox/flox};Rosa26^{L\text{-}S\text{-}L\text{-}Luc/+}$ mice and bioluminescence imaging (BLI) was used to monitor tumor response to rapamycin therapy over a one month course of treatment. Two tumor-bearing mice were treated with rapamycin (1mg/kg) and two were treated with vehicle. BLI was carried out just prior to initiation of treatment 6 weeks after ovarian bursal injection of AdCre, and weekly for one month thereafter (Figures 5E,F). Both vehicle-treated animals showed a substantial increase in tumor bioluminescence over the treatment interval, while bioluminescence in the rapamycin-treated mice increased only minimally in one mouse (Rap1) and decreased in the other mouse (Rap2). Comparison of tumor volume and BLI signal at study endpoint is shown in Figure 5G.

MEK/ERK signaling is up-regulated in response to AKT inhibition in murine APC^{-}/PTEN^{-} and human ovarian carcinoma cell lines

Recent findings imply a link between mTOR inhibition and ERK activation, possibly reflecting interruption of an S6K1-dependent negative feedback loop (29, 30). Moreover, simultaneous inhibition of mTOR and MEK/ERK signaling has been shown to substantially enhance anti-tumor effects in vitro and in vivo (31, 32). We tested whether inhibition of AKT signaling in murine and human ovarian cancer cell lines is associated with compensatory up-regulation of MEK/ERK signaling. As expected, perifosine treatment for 2 hr resulted in a dose-dependent reduction of pAKT and pS6 in W2671T, W2830T and A2780 cells (Figure 6A, B). Notably, pERK was also substantially increased in all three cell lines following treatment with perifosine. Similar findings were noted in cells treated with API-2, including A2780 cells with and without mutant (S33Y) β-catenin (Figure 6C,D). Up-regulation of MEK/ERK signaling was also observed in rapamycin treated W2830T and TOV-112D cell lines (Figures 6E and S2A).

DISCUSSION

Thus far, clinical trials of new drugs have relied heavily on preclinical studies testing drug effects on OvCa-derived cell lines in culture or xenografted into immune-compromised mice. These systems have a number of shortcomings, reviewed by Frese and Tuveson among others (33), and there is hope that genetically engineered mouse (GEM) models of OvCa will prove superior to cultured cells and tumor xenografts for testing the efficacy of novel therapeutic regimens. Existing GEM models of OvCa have been surprisingly underutilized for this purpose. In the studies presented here we have focused on addressing the utility of a robust mouse OEA model, based on conditional inactivation of the *Apc* and *Pten* tumor suppressor genes in the ovarian surface epithelium, for pre-clinical testing of agents targeting activated PI3K/AKT/mTOR signaling.

Although many OEAs are low-stage at diagnosis and have an excellent prognosis, a substantial fraction of OEAs present at FIGO stage III or IV. Based on a series of cases from which data were prospectively collected over a 20 year period at a single center, 48% were high stage at diagnosis and these were associated with poor (less than 12%) 5-year progression-free survival after platinum-based therapy (34). It is reasonable to hope that drugs which target activated PI3K/Akt/mTOR signaling might prove to be useful for treating patients whose tumors harbor mutations that dysregulate this signaling pathway, particularly those with high stage disease or risk of recurrence. Given the modest number of patients with OEAs and the many drug combinations, doses, and schedules that could be explored in clinical trials, we hypothesized that our mouse OEA model might prove valuable for validating the concept of targeting PI3K/AKT/mTOR signaling in OEAs and in defining a limited number of higher priority agents and combinations. We report data here showing that agents targeting PI3K/AKT/mTOR signaling are active in vitro and in vivo against OEAs, and that longitudinal imaging approaches with luciferase-based reporters to measure tumor burden and dissemination might be particularly promising.

Platinum-taxane combination chemotherapy is well established as first-line therapy for advanced ovarian cancer, including OEAs (35). Initial response rates exceed 80%, but most patients relapse and response of recurrent disease to other agents such as doxorubicin, gemcitabine, topotecan, and etoposide is unpredictable. Moreover, the likelihood of response decreases with each subsequent relapse. Attempts to overcome chemoresistance following platinum/taxane therapy using different classes of chemotherapeutic agents in various combinations, doses, and schedules have led to only incremental improvements in overall survival. More recently, improved understanding of ovarian cancer biology and molecular genetics has led to the development of targeted therapies, several of which have

been tested in clinical trials. These include agents that target angiogenesis, Erbb family members such as EGFR and ERBB2, and α-FR (reviewed by Yap et al.) (35). Although the PI3K/Akt/mTOR signaling pathway is frequently activated in human ovarian cancers, including OEAs as discussed above, clinical trials assessing the potential of PI3K, Akt, or mTOR inhibitors for treating ovarian cancer have been somewhat limited thus far. In a small (15 subject) phase I study of weekly temsirolimus (mTOR inhibitor also known as CCI-779) and topotecan for treatment of advanced or recurrent gynecologic malignancies - nearly half of which were ovarian cancers - there were no complete or partial responses. Furthermore, myelosuppression was found to be dose-limiting for the combination, and patients who had received prior pelvic radiation were unable to tolerate the treatment (36). A phase II trial assessing temsirolimus as a single agent in patients with persistent or recurrent ovarian cancer showed modest effects, but progression free survival was below the level that would warrant phase III studies in unselected patients (37). Interestingly, a phase II study of another mTOR inhibitor, everolimus, has shown encouraging results as a single agent for patients with recurrent endometrioid adenocarcinomas of the endometrium (38), which like OEAs, have frequent mutations that dysregulate PI3K/Akt/mTOR signaling. Our data, using both in vitro and in vivo model systems, suggest that Akt and mTOR inhibitors are likely to have efficacy for treating ovarian cancers with PI3K/Akt/mTOR pathway defects. Santiskulvong and colleagues recently showed that dual targeting of PI3K and mTOR inhibited growth of ovarian carcinomas arising in another murine GEM model based on conditional activation of a mutant *K-ras* allele and biallelic inactivation of *Pten* (39). Collectively, our data provide support for using GEM models of ovarian cancer to help pre-select drug regimens with greatest promise for efficacy in human clinical trials. For example, such models could be used to help determine whether a given targeted agent is likely to be more effective given simultaneously with, or after conventional therapy. Toxicities likely to be dose-limiting could also be identified.

A number of different modalities have been employed to non-invasively image tumors in living animals, including those developing in the context of GEM models. These modalities include high resolution ultrasound (40), micro-computed tomography (micro-CT) (41), micro-positron emission tomography (micro-PET) (42), magnetic resonance imaging (MRI) (43), and BLI (44, 45). Although each modality has pros and cons, some of the advantages of BLI include its high sensitivity, relatively low cost, short image acquisition times and relative ease of use with minimal image post-processing requirements (44). Our model system has been engineered such that the luciferase reporter is synchronously activated when *Pten* and *Apc* are inactivated, allowing tumors to be monitored longitudinally over time with BLI, essentially from their inception. We have also shown that BLI can be effectively used to monitor effects of therapy.

The PI3K/AKT/mTOR and MEK/ERK signaling pathways likely cooperate in many tumor types to drive tumor growth, promote tumor cell survival and mediate resistance to therapy. Simultaneous inhibition of both pathways with targeted agents has been shown to substantially enhance anti-tumor effects in vitro and in vivo (31, 32, 46). Similar to our findings in OEA-derived cell lines, Rahmani and colleagues showed that treatment of leukemia cells with perifosine, which inhibits PI3K/Akt/mTOR signaling upstream of mTORC1, also induced Erk activation (47). Notably, combined treatment with the Mek inhibitor PD184352 and perifosine strikingly induced apoptosis in multiple malignant human hematopoietic cells. Although effects of Akt and mTOR inhibition on Erk activation may vary with cell type and context, our data suggest that clinical trials involving the use of targeted agents for ovarian cancers with activated PI3K/Akt/mTOR signaling should focus not only on improving the activity of conventional cytotoxic drugs by combining them with targeted agents, but also on designing rational combinations of targeted agents that inhibit complementary or compensatory cell survival pathways. We anticipate that animal models

such as the one described here should facilitate identification of the most successful combination therapies for subsequent evaluation in clinical trials.

Supplementary Material

Refer to Web version on PubMed Central for supplementary material.

Acknowledgments

This work was supported by grants from the National Cancer Institute (RO1 CA4172) and the Department of Defense Ovarian Cancer Research Program (W81XWH-08-1-0453).

References

1. Seidman JD, Horkayne-Szakaly I, Haiba M, Boice CR, Kurman RJ, Ronnett BM. The histologic type and stage distribution of ovarian carcinomas of surface epithelial origin. Int J Gynecol Pathol. 2004; 23:41–4. [PubMed: 14668549]
2. Jemal A, Siegel R, Xu J, Ward E. Cancer statistics, 2010. CA Cancer J Clin. 2010; 60:277–300. [PubMed: 20610543]
3. Kurman RJ, Shih IeM. Pathogenesis of ovarian cancer: lessons from morphology and molecular biology and their clinical implications. Int J Gynecol Pathol. 2008; 27:151–60. [PubMed: 18317228]
4. Shih, IeM; Kurman, RJ. Ovarian tumorigenesis: a proposed model based on morphological and molecular genetic analysis. Am J Pathol. 2004; 164:1511–8. [PubMed: 15111296]
5. Seidman, JD.; Cho, KR.; Ronnett, BM.; Kurman, RJ. Surface Epithelial Tumors of the Ovary. In: Kurman, RJ.; Ellenson, LH.; Ronnett, BM., editors. Blaustein's Pathology of the Female Genital Tract. 6. New York: Springer; 2011.
6. Ahmed AA, Etemadmoghadam D, Temple J, Lynch AG, Riad M, Sharma R, et al. Driver mutations in TP53 are ubiquitous in high grade serous carcinoma of the ovary. J Pathol. 2010; 221:49–56. [PubMed: 20229506]
7. Wu R, Hendrix-Lucas N, Kuick R, Zhai Y, Schwartz DR, Akyol A, et al. Mouse model of human ovarian endometrioid adenocarcinoma based on somatic defects in the Wnt/B-catanin and PI3K/Pten signaling pathways. Cancer Cell. 2007; 11:321–33. [PubMed: 17418409]
8. Cho KR, Shih IM. Ovarian Cancer. Annu Rev Pathol Mech Dis. 2009; 4:287–313.
9. McCluggage WG. My approach to and thoughts on the typing of ovarian carcinomas. J Clin Pathol. 2008; 61:152–63. [PubMed: 17704261]
10. Wiegand KC, Shah SP, Al-Agha OM, Zhao Y, Tse K, Zeng T, et al. ARID1A mutations in endometriosis-associated ovarian carcinomas. N Engl J Med. 2010; 363:1532–43. [PubMed: 20942669]
11. Shibata H, Toyama K, Shioya H, Ito M, Hirota M, Hasegawa S, et al. Rapid colorectal adenoma formation initiated by conditional targeting of the Apc gene. Science. 1997; 278:120–3. [PubMed: 9311916]
12. Suzuki A, Yamaguchi MT, Ohteki T, Sasaki T, Kaisho T, Kimura Y, et al. T cell-specific loss of Pten leads to defects in central and peripheral tolerance. Immunity. 2001; 14:523–34. [PubMed: 11371355]
13. Roby KF, Taylor CC, Sweetwood JP, Cheng Y, Pace JL, Tawfik O, et al. Development of a syngeneic mouse model for events related to ovarian cancer. Carcinogenesis. 2000; 21:585–91. [PubMed: 10753190]
14. Wu R, Zhai Y, Fearon ER, Cho KR. Diverse Mechanisms of beta-Catenin Deregulation in Ovarian Endometrioid Adenocarcinomas. Cancer Res. 2001; 61:8247–55. [PubMed: 11719457]
15. Saito M, Okamoto A, Kohno T, Takakura S, Shinozaki H, Isonishi S, et al. Allelic imbalance and mutations of the PTEN gene in ovarian cancer. Int J Cancer. 2000; 85:160–5. [PubMed: 10629071]

16. Kolligs FT, Hu G, Dang CV, Fearon ER. Neoplastic transformation of RK3E by mutant beta-catenin requires deregulation of Tcf/Lef transcription but not activation of c-myc expression. Mol Cell Biol. 1999; 19:5696–706. [PubMed: 10409758]

17. Safran M, Kim WY, Kung AL, Horner JW, DePinho RA, Kaelin WG Jr. Mouse reporter strain for noninvasive bioluminescent imaging of cells that have undergone Cre-mediated recombination. Mol Imaging. 2003; 2:297–302. [PubMed: 14717328]

18. Mandai M, Yamaguchi K, Matsumura N, Baba T, Konishi I. Ovarian cancer in endometriosis: molecular biology, pathology, and clinical management. Int J Clin Oncol. 2009; 14:383–91. [PubMed: 19856044]

19. Hideshima T, Catley L, Yasui H, Ishitsuka K, Raje N, Mitsiades C, et al. Perifosine, an oral bioactive novel alkylphospholipid, inhibits Akt and induces in vitro and in vivo cytotoxicity in human multiple myeloma cells. Blood. 2006; 107:4053–62. [PubMed: 16418332]

20. Choo AY, Blenis J. Not all substrates are treated equally: implications for mTOR, rapamycin-resistance and cancer therapy. Cell Cycle. 2009; 8:567–72. [PubMed: 19197153]

21. Dowling RJ, Topisirovic I, Fonseca BD, Sonenberg N. Dissecting the role of mTOR: lessons from mTOR inhibitors. Biochim Biophys Acta. 2010; 1804:433–9. [PubMed: 20005306]

22. Chen XG, Liu F, Song XF, Wang ZH, Dong ZQ, Hu ZQ, et al. Rapamycin regulates Akt and ERK phosphorylation through mTORC1 and mTORC2 signaling pathways. Mol Carcinog. 2010; 49:603–10. [PubMed: 20512842]

23. Sarbassov DD, Ali SM, Sengupta S, Sheen JH, Hsu PP, Bagley AF, et al. Prolonged rapamycin treatment inhibits mTORC2 assembly and Akt/PKB. Mol Cell. 2006; 22:159–68. [PubMed: 16603397]

24. She QB, Halilovic E, Ye Q, Zhen W, Shirasawa S, Sasazuki T, et al. 4E-BP1 is a key effector of the oncogenic activation of the AKT and ERK signaling pathways that integrates their function in tumors. Cancer Cell. 2010; 18:39–51. [PubMed: 20609351]

25. Inoki K, Ouyang H, Zhu T, Lindvall C, Wang Y, Zhang X, et al. TSC2 integrates Wnt and energy signals via a coordinated phosphorylation by AMPK and GSK3 to regulate cell growth. Cell. 2006; 126:955–68. [PubMed: 16959574]

26. Yang L, Dan HC, Sun M, Liu Q, Sun XM, Feldman RI, et al. Akt/protein kinase B signaling inhibitor-2, a selective small molecule inhibitor of Akt signaling with antitumor activity in cancer cells overexpressing Akt. Cancer Res. 2004; 64:4394–9. [PubMed: 15231645]

27. Fu L, Kim YA, Wang X, Wu X, Yue P, Lonial S, et al. Perifosine inhibits mammalian target of rapamycin signaling through facilitating degradation of major components in the mTOR axis and induces autophagy. Cancer Res. 2009; 69:8967–76. [PubMed: 19920197]

28. Beuvink I, Boulay A, Fumagalli S, Zilbermann F, Ruetz S, O'Reilly T, et al. The mTOR inhibitor RAD001 sensitizes tumor cells to DNA-damaged induced apoptosis through inhibition of p21 translation. Cell. 2005; 120:747–59. [PubMed: 15797377]

29. Grant S. Cotargeting survival signaling pathways in cancer. J Clin Invest. 2008; 118:3003–6. [PubMed: 18725993]

30. Aksamitiene E, Kholodenko BN, Kolch W, Hoek JB, Kiyatkin A. PI3K/Akt-sensitive MEK-independent compensatory circuit of ERK activation in ER-positive PI3K-mutant T47D breast cancer cells. Cell Signal. 2010; 22:1369–78. [PubMed: 20471474]

31. Carracedo A, Ma L, Teruya-Feldstein J, Rojo F, Salmena L, Alimonti A, et al. Inhibition of mTORC1 leads to MAPK pathway activation through a PI3K-dependent feedback loop in human cancer. J Clin Invest. 2008; 118:3065–74. [PubMed: 18725988]

32. Kinkade CW, Castillo-Martin M, Puzio-Kuter A, Yan J, Foster TH, Gao H, et al. Targeting AKT/mTOR and ERK MAPK signaling inhibits hormone-refractory prostate cancer in a preclinical mouse model. J Clin Invest. 2008; 118:3051–64. [PubMed: 18725989]

33. Frese KK, Tuveson DA. Maximizing mouse cancer models. Nat Rev Cancer. 2007; 7:645–58. [PubMed: 17687385]

34. Storey DJ, Rush R, Stewart M, Rye T, Al-Nafussi A, Williams AR, et al. Endometrioid epithelial ovarian cancer : 20 years of prospectively collected data from a single center. Cancer. 2008; 112:2211–20. [PubMed: 18344211]

35. Yap TA, Carden CP, Kaye SB. Beyond chemotherapy: targeted therapies in ovarian cancer. Nat Rev Cancer. 2009; 9:167–81. [PubMed: 19238149]
36. Temkin SM, Yamada SD, Fleming GF. A phase I study of weekly temsirolimus and topotecan in the treatment of advanced and/or recurrent gynecologic malignancies. Gynecol Oncol. 2010; 117:473–6. [PubMed: 20347480]
37. Behbakht K, Sill MW, Darcy KM, Rubin SC, Mannel RS, Waggoner S, et al. Phase II trial of the mTOR inhibitor, temsirolimus and evaluation of circulating tumor cells and tumor biomarkers in persistent and recurrent epithelial ovarian and primary peritoneal malignancies: A Gynecologic Oncology Group study. Gynecol Oncol. 2011
38. Slomovitz BM, Lu KH, Johnston T, Coleman RL, Munsell M, Broaddus RR, et al. A phase 2 study of the oral mammalian target of rapamycin inhibitor, everolimus, in patients with recurrent endometrial carcinoma. Cancer. 2010; 116:5415–9. [PubMed: 20681032]
39. Santiskulvong C, Konecny GE, Fekete M, Chen KY, Karam A, Mulholland D, et al. Dual Targeting of Phosphoinositide 3-Kinase and Mammalian Target of Rapamycin Using NVP-BEZ235 as a Novel Therapeutic Approach in Human Ovarian Carcinoma. Clin Cancer Res. 2011; 17:2373–84. [PubMed: 21372221]
40. Cook N, Olive KP, Frese K, Tuveson DA. K-Ras-driven pancreatic cancer mouse model for anticancer inhibitor analyses. Methods Enzymol. 2008; 439:73–85. [PubMed: 18374157]
41. Singh M, Lima A, Molina R, Hamilton P, Clermont AC, Devasthali V, et al. Assessing therapeutic responses in Kras mutant cancers using genetically engineered mouse models. Nat Biotechnol. 2010; 28:585–93. [PubMed: 20495549]
42. Pestourie C, Theze B, Kuhnast B, Le Helleix S, Gombert K, Dolle F, et al. PET imaging of medullary thyroid carcinoma in MEN2A transgenic mice using 6-[(18)F]F-L-DOPA. European journal of nuclear medicine and molecular imaging. 2010; 37:58–66. [PubMed: 19655139]
43. Hensley H, Quinn BA, Wolf RL, Litwin SL, Mabuchi S, Williams SJ, et al. Magnetic resonance imaging for detection and determination of tumor volume in a genetically engineered mouse model of ovarian cancer. Cancer Biol Ther. 2007; 6:1717–25. [PubMed: 17986851]
44. O'Neill K, Lyons SK, Gallagher WM, Curran KM, Byrne AT. Bioluminescent imaging: a critical tool in pre-clinical oncology research. J Pathol. 2010; 220:317–27. [PubMed: 19967724]
45. Connolly DC, Hensley HH. Xenograft and Transgenic Mouse Models of Epithelial Ovarian Cancer and Non Invasive Imaging Modalities to Monitor Ovarian Tumor Growth In situ - Applications in Evaluating Novel Therapeutic Agents. Curr Protoc Pharmacol. 2009; 45:14.12.1–14.12.26. [PubMed: 20634901]
46. Villanueva J, Vultur A, Lee JT, Somasundaram R, Fukunaga-Kalabis M, Cipolla AK, et al. Acquired resistance to BRAF inhibitors mediated by a RAF kinase switch in melanoma can be overcome by cotargeting MEK and IGF-1R/PI3K. Cancer Cell. 2010; 18:683–95. [PubMed: 21156289]
47. Rahmani M, Anderson A, Habibi JR, Crabtree TR, Mayo M, Harada H, et al. The BH3-only protein Bim plays a critical role in leukemia cell death triggered by concomitant inhibition of the PI3K/Akt and MEK/ERK1/2 pathways. Blood. 2009; 114:4507–16. [PubMed: 19773546]

STATEMENT OF TRANSLATIONAL RELEVANCE

Currently available therapies have improved survival for patients with advanced ovarian carcinoma, but many patients ultimately relapse and die from their cancer. There is great interest in designing new “individualized” therapeutic regimens based on the specific molecular defects present in a given patient’s tumor. Although many drugs and drug combinations are potentially available, identification of the most efficacious of these remains a challenging process that cannot easily be conducted in women with the disease. We have demonstrated the pre-clinical utility of a genetically engineered mouse model of ovarian carcinoma that closely resembles human endometrioid ovarian cancers with Wnt and PI3K/AktT/mTOR pathway defects for comparison of the activities of multiple drugs targeting activated PI3K/Akt/mTOR signaling. The data suggest the mouse model strategy described here should help accelerate the transition of the most promising new therapies from the laboratory into clinical trials.

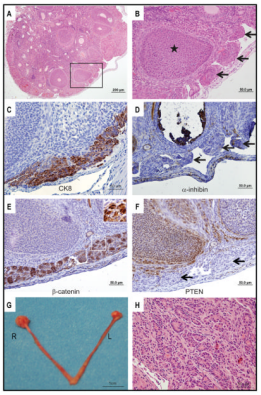

Figure 1. Murine OEA-like tumors arise within 3 weeks of ovarian bursal AdCre injection in *Apc*$^{flox/flox}$;*Pten*$^{flox/flox}$ mice

A) Low magnification photomicrograph of H&E stained section from right ovary 3 weeks after AdCre injection showing multifocal “tumorlets” on the ovarian surface. B) High magnification photomicrograph of the boxed area in panel A showing “tumorlets” (arrows) and ovarian follicle (star). Tissue sections were IHC stained for C) cytokeratin 8; D) α-inhibin; E) β-catenin; and F) PTEN. Cells in the surface tumorlets are positive for cytokeratin 8 and show strong nuclear staining for β-catenin. The tumor cells are negative for α-inhibin and PTEN (arrows indicate tumorlets). G) Gross photograph of upper genital tract 6 weeks after AdCre injection of right ovarian bursa shows modestly enlarged right (R) ovary relative to the control left (L) ovary. H) Photomicrograph of H&E stained section from ovarian tumor present 6 weeks after AdCre injection. Areas of overt glandular differentiation are admixed with poorly differentiated and spindle cell areas.

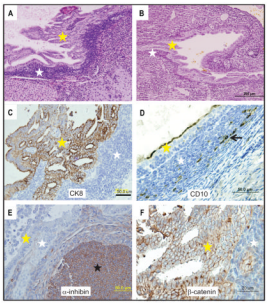

Figure 2. Endometriosis-like lesions are present in the ovaries of *Apc*$^{flox/flox}$ mice

Photomicrographs of H&E stained sections from the A) right and B) left ovaries of *Apc*$^{flox/flox}$ mice 12 months after AdCre injection showing endometriosis-like lesions with endometrial-type glands (yellow stars) and adjacent stroma (white stars). Tissue sections with endometriosis were IHC stained for C) cytokeratin 8, D) CD10, E) α-inhibin, and F) β-catenin. The glandular epithelium (yellow stars) is strongly positive for cytokeratin 8, negative for α-inhibin, and shows membranous staining for β-catenin. The adjacent stroma shows focal CD10 positivity (black arrow) and is only weakly positive forα-inhibin compared to granulosa cells in the ovarian follicle (black star).

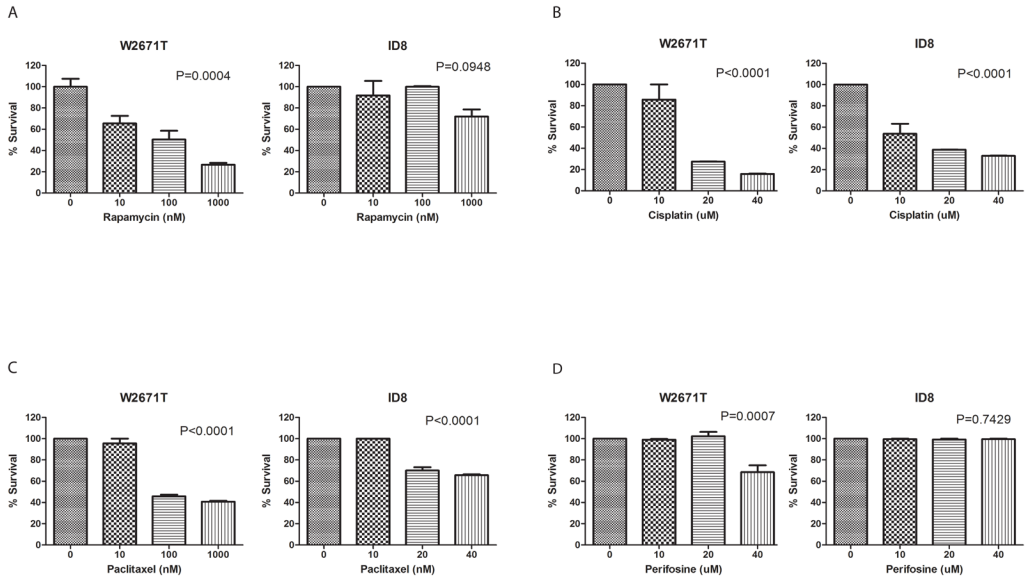

Figure 3. Status of PI3K/AKT/mTOR signaling in murine ovarian cancer cells determines response to Akt and mTOR inhibitors, but not to conventional cytotoxic drugs

Growth inhibitory effects of A) rapamycin, B) cisplatin, C) paclitaxel, and D) perifosine were evaluated in W2671T, W2830T and ID8 cells in vitro. After exposure to indicated drugs or controls for 24 hr, cell viability was measured with WST-1 reagent. Proportional viability (%) was calculated by comparing the drugs with vehicle controls, whose viability was assumed to be 100%. Values represent the average of three independent assays performed in duplicate, expressed as means ± SD. Differences between control and treated cells were analyzed by one way ANOVA.

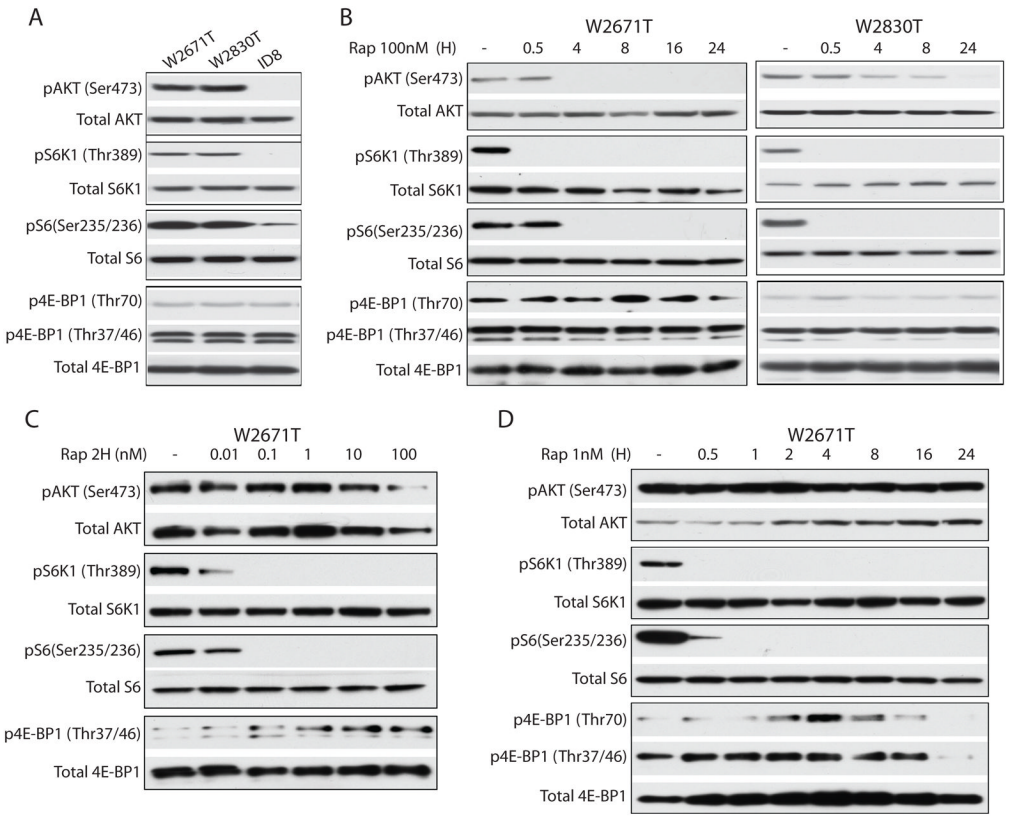

Figure 4. Characterization of PI3K/AKT/mTOR signaling pathway regulation in murine ovarian cancer cells after treatment with mTOR or Akt inhibitors

Immunoblots showing A) Endogenous levels of phosphorylated and total Akt, S6K1, S6, and 4E-BP1 in W2671T, W2830T and ID8 cells. B) Time course of high dose (100nM) rapamycin treatment of W2671T and W2830T cell lines. Phosphorylated and total Akt, S6K1, S6, and 4E-BP1 are shown. C) Dose-dependent effect of rapamycin (0.01nM to 100nM) on phosphorylation of Akt, S6K1, S6, and 4E-BP1 after exposure to rapamycin for 2 hr in W2671T. D) Time course of low dose (1nM) rapamycin treatment of W2671T cells. Phosphorylated and total Akt, S6K1, S6, and 4E-BP1 are shown.

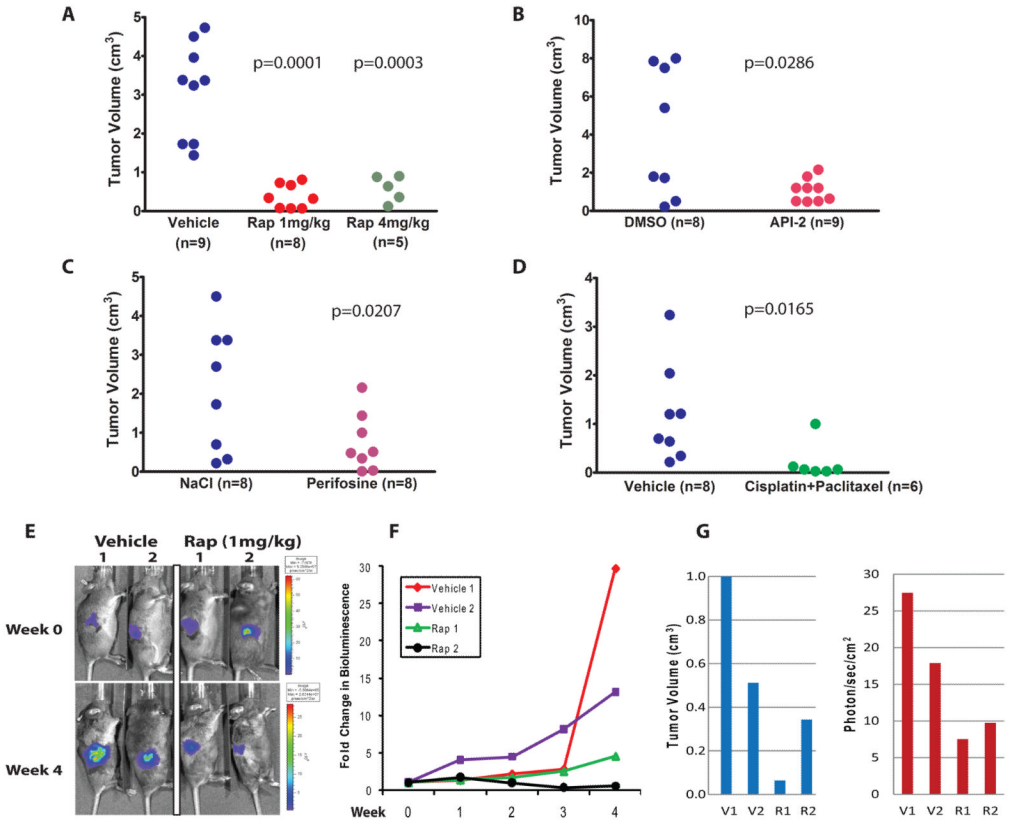

Figure 5. Inhibition of APC^{-}/PTEN^{-} murine ovarian tumor growth in vivo by conventional chemotherapy and drugs targeting activated PI3K/Akt/mTOR signaling

Small ovarian tumors present 6 weeks after AdCre injection were treated for 4 weeks with vehicle or A) rapamycin (1mg/kg and 4mg/kg), B) API-2, C) perifosine, or D) cisplatin plus paclitaxel. Mice were euthanized at the end of the treatment period and right ovarian tumor volume was measured (length X width X height) using calipers. All treated groups showed significantly smaller tumors than controls. P values from two-sample t tests on tumor volume are shown. E) Bioluminescence imaging was performed weekly in tumor bearing animals treated with vehicle or rapamycin. Treatment was initiated 6 weeks after AdCre injection of the right ovarian bursae of *Apc$^{flox/flox}$;Pten$^{flox/flox}$; ROSA26 $^{L\text{-}S\text{-}L\text{-}luc/+}$* mice. Representative images before and after 4 weeks of treatment with rapamycin or vehicle are shown. Bioluminescence is indicated as photons/second/cm^2. Red signals correspond to maximal intensity, violet to minimal intensity and other colors representing values in between. F) Graph showing fold-change in luciferase activity based on BLI imaging of vehicle versus rapamycin treated animals over the 4 week treatment course. G) Comparison of tumor volume and BLI signal at study endpoint in vehicle and rapamycin treated animals.

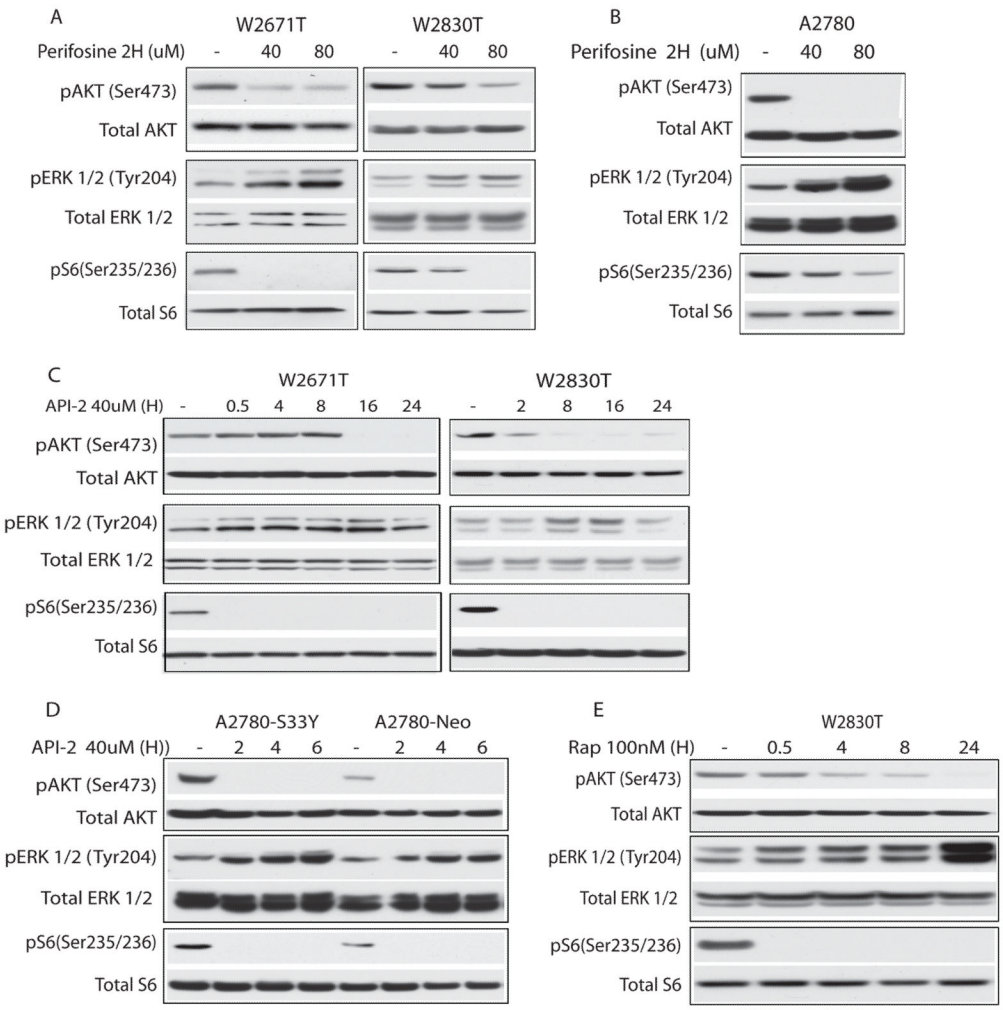

Figure 6. Akt inhibition in murine and human ovarian tumor cells results in compensatory activation of MEK/ERK signaling

Immunoblots of lysates from A) W2671T and W2830T and B) A2780 cells treated for 2 hr with varying doses of perifosine; C) W2671T and W2830T and D) A2780-S33Y and A2780-Neo cells treated with 40 μM API-2 over the indicated time course; E) W2830T cells treated with 100nM rapamycin for up to 24 hr. In each blot, levels of phosphorylated and total Akt, ERK, and S6 are shown.

Table 1

Ovarian Tumor Development Following AdCre Injection

Week	Number of Mice	Microscopic Tumor	Macroscopic Tumor	% with Tumor
1	2	0	0	0
2	8	0	0	0
3	10	6	0	60
4	7	6	0	85.7
5	3	3	0	100
6	13	2	11	100

Table 2

Drug Response of Murine APC^{-}/PTEN^{-} Ovarian Cancers

Drug	Tumor Volume (cm^3) (Mean ± SD)	Liver Metastasis	Ascites
Rapamycin (4mg/kg)	0.581 ± 0.336	0/5	0/5
Rapamycin (1mg/kg)	0.386 ± 0.311	0/8	2/8
Vehicle	3.12 ± 1.226	2/9	5/9
API-2	1.078 ± 0.201	0/9	0/9
DMSO	4.126 ± 1.205	0/8	3/8
Perifosine	0.746 ± 0.263	0/8	0/8
NaCl	2.116 ± 0.569	1/8	1/8
Cisplatin + paclitaxel	0.218 ± 0.157	0/6	0/6
NaCl + DMSO	1.199 ± 0.357	0/8	3/8